Cement and Concrete Research 39 (2009) 1033–1043

Contents lists available at ScienceDirect

Cement and Concrete Research

journal homepage: http://ees.elsevier.com/CEMCON/default.asp

Durability properties of micro-cracked ECC containing high volumes fly ash

Mustafa Şahmaran [a], Victor C. Li [b,*]

[a] Department of Civil Engineering, Gaziantep University, 27310, Gaziantep, Turkey
[b] Department of Civil and Environmental Engineering, The University of Michigan, Ann Arbor, MI, 48109, United States

ARTICLE INFO

Article history:
Received 24 May 2008
Accepted 15 July 2009

Keywords:
Microcracking (B)
Durability (C)
Fly ash (D)
Self-healing

ABSTRACT

This paper presents the durability of Engineered Cementitious Composites (ECC) that contain high percentages of Class-F fly ash (FA). ECC is a newly developed high performance fiber reinforced cementitious composite with substantial benefit in both high ductility in excess of 3% under uniaxial tensile loading and improved durability due to intrinsically tight crack width. Composites containing two different contents of FA as a replacement of cement (55 and 70% by weight of total cementitious material) are examined after 28 days of curing. Accelerated aging (exposure to continuous sodium hydroxide at 38 °C and sodium chloride solutions at room temperature) and tests of transport properties (salt ponding, rapid chloride permeability and sorptivity tests) are used to study the effect of FA on the durability of the ECC. After accelerated aging, direct tensile tests are performed to evaluate the effect of deterioration on the tensile strength, tensile strain capacity and crack width of ECCs. In addition to virgin specimens, the durability performances of mechanically loaded specimens are also tested. Test results show that both mechanically pre-loaded and virgin (without pre-loading) ECC mixtures with high volumes of FA remain durable in terms of mechanical performances after accelerated aging period, and show a tensile strain capacity of more than 2%. In terms of transport properties, micro-cracks induced by mechanical pre-loading increase the chloride transport and the sorptivity values of ECC. Moreover, increasing FA content is shown to have a negative effect especially on the transport properties of ECC tested in this study. However, the risk of water transport by capillary suction and chloride transport by diffusion in ECC, cracked or uncracked, is found to be comparable with that in normal sound concrete.

1. Introduction

Mineral admixtures such as silica fume (SF), fly ash (FA) and ground granulated blast furnace slag (GBFS) generally improve the engineering properties of concrete when they are used as a mineral additive or partial replacement of cement. Among these mineral admixtures, FA is a finely divided residue that is a by-product from the combustion of powdered coal in power plants. FA has been used in concrete production for over 50 years in the world. It was used in mass, conventional and high performance concrete to improve the workability, to reduce the heat of hydration and thermal cracking at early ages, and to improve the mechanical and durability properties especially at later ages.

Engineered Cementitious Composites (ECC) is a new class of HPFRCC micro-mechanically designed to achieve high damage tolerance under severe loading and high durability under normal service conditions [1–3]. Unlike ordinary concrete materials, ECC strain-hardens after first cracking, similar to a ductile metal, and demonstrates a strain capacity 300–500 times greater than normal concrete (Fig. 1). Along with tensile ductility, the unique crack development within ECC is critical to its durability. Different from ordinary concrete and most fiber reinforced concretes (FRC), ECC exhibits self-controlled crack widths under increasing load (Fig. 1). After initial loading, a small number of cracks form within the material and begin to widen. This widening continues until they have reached an average width of about 60 μm, at approximately 1% strain. Following this, the initial cracks do not widen further as additional tensile deformation is accommodated by the formation of new micro-cracks until the material is saturated with these cracks, with spacing about 1–2 mm. Regardless of the ultimate tensile strain, average crack widths remain at about 60 μm. This is only possible through the formation of steady-state "flat cracks" which exhibit a constant crack width independent of crack length, in contrast to Griffith-type cracks present in most FRC and HPFRCC materials which widen as the crack grows [1–3]. The formation of steady-state cracking is the result of micro-mechanical tailoring of ECC material.

Recently, various investigations have focused on the durability performance of a widely studied "standard" ECC mixture, known also as ECC M45, that has a fly ash–cement ratio of 1.2, by weight [4–12]. As a result of these investigations, it has been shown that the standard ECC mixture is highly durable under accelerated weathering tests [6,12], freeze–thaw cycles with/without de-icing salts [4,10] and reinforcement corrosion [7]. Furthermore, micro-cracked ECC exhibits

* Corresponding author. Tel.: +1 734 764 3368; fax: +1 734 764 4292.
E-mail address: vcli@umich.edu (V.C. Li).

0008-8846/$ – see front matter © 2009 Elsevier Ltd. All rights reserved.
doi:10.1016/j.cemconres.2009.07.009

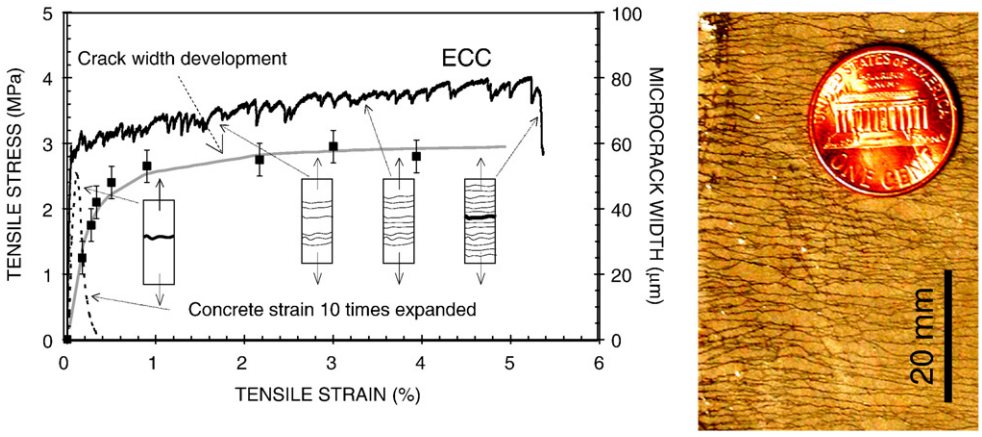

Fig. 1. Typical tensile stress–strain curve and crack width development of ECC.

nearly the same transport properties as sound concrete, even when strained in tension to several percent.

Recently, fly ash (FA) has become what some consider a necessary component of ECC [4,13,14]. Increasing the amount of FA (up to 85% replacement by weight of cement content) in high volume FA (HVFA) ECC tends to improve robustness of tensile ductility while retaining a long-term tensile strain of approximately 3% [4,13,14]. Moreover, with an increase of the FA amount, the crack width is reduced from about 60 μm level to 10–30 μm level or sometimes even lower than 10 μm level, which may benefit the long-term durability of HVFA–ECC structures. The improvement in the tensile strain and crack width with the increase in the FA content can be attributed to the fact that the increase in the FA content tends to reduce the fiber/matrix interface chemical bond and matrix toughness, while increasing the interface frictional bond, in favor of attaining high tensile strain capacity [14]. As briefly mentioned above, several studies have addressed the durability properties of standard ECC mixture (M45) with the average crack widths about 60 μm after tensile loading, but no research work so far has been reported on the durability properties of the newer version HVFA–ECC with tighter crack width. Therefore, the objective of this research is to assess the effect of FA on the durability properties of HVFA–ECC. ECC mixtures with two different fly ash–Portland cement (FA/PC) ratios (1.2 and 2.2 by weight) were prepared. After various numbers of micro-cracks were introduced to the ECC beam and coupon specimens by mechanical pre-loading, water sorptivity, chloride penetration tests and accelerated aging were performed to develop an understanding of the influence of FA/PC ratio (with associated micro-crack widths) on durability characteristics.

2. Experimental studies

2.1. Materials and mixture proportions

The materials used in ECC mixtures were ordinary Portland cement (PC), Class-F fly ash (FA), silica sand with average and maximum grain sizes of 110 μm and 200 μm respectively, water, poly-vinyl alcohol (PVA) fibers, and a high range water reducing admixture (HRWR). The physical properties and chemical compositions of the FA and PC are listed in Table 1. The PVA fibers with a diameter of 39 μm, a length of 8 mm are purposely manufactured with a tensile strength (1620 MPa), elastic modulus (42.8 GPa), and maximum elongation (6.0%) matching those needed for strain-hardening performance. Additionally, the surface of the PVA fibers is coated with a proprietary oiling agent 1.2% by weight to tailor the interfacial properties between fiber and matrix for strain-hardening performance [15].

Details of the two ECC mixtures, with FA/PC of 1.2 and 2.2 by weight, used in this investigation are given in Table 2. The ECC mixtures were prepared in a standard mortar mixer at a constant amount of cementitious material and constant water to cementitious material (W/CM) ratio of 0.27. HRWR was added to the mixture until the desired fresh ECC characteristics were visually observed.

The compressive strength of the two ECC mixtures at the ages of 7, 28 and 90 days is also listed in Table 2. A minimum of three compression cylinders (75 mm diameter by 150 mm height) was used to obtain the average compressive strengths, following ASTM C39 procedures. As seen from Table 3 and as expected, the compressive strength of ECC decreased with increasing FA content. However even at almost 70% replacement of Portland cement with FA (FA/PC = 2.2), the compressive strength of ECC at 28 days can be more than 35 MPa.

2.2. Specimen preparation and testing

From each mixture, 355 × 50 × 75 mm prism specimens were prepared for salt ponding and sorptivity tests, and 100 × 200-mm cylinder specimens were prepared for rapid chloride permeability test (RCPT). In addition, 152.4 × 76.2 × 12.7 mm coupon specimens were prepared for the direct uniaxial tensile test for the ECC mixtures under different exposure conditions. All specimens were demolded at the age of 24 h, and cured in sealed plastic bag at 95 ± 5% RH, 23 ± 2 °C for 7 days. The specimens were then air cured at 50 ± 5% RH, 23 ± 2 °C until the age of 28 days for testing. The complete testing program is detailed below.

2.2.1. Salt ponding and rapid chloride permeability tests (RCPT)

Chloride ion profiles and diffusion coefficient of ECC was evaluated in accordance with AASHTO T259-80 [16]. At the age of 28 days, prisms surface were abraded using a steel brush as required by

Table 1
Physical properties and chemical compositions of FA and PC.

Chemical composition	FA	PC	Physical properties	FA	PC
SiO_2, %	55.71	19.61	Moisture content, %	0.16	–
Al_2O_3, %	22.56	5.86	Loss on ignition, %	0.41	3.02
Fe_2O_3, %	5.61	3.40	Amount retained on #325 sieve, %	23.63	–
Sum, %	83.88	28.87	Specific gravity	2.29	3.18
CaO, %	10.44	63.27	Autoclave soundness, %	0.02	–
MgO, %	1.78	0.95	Strength activity index w/	77.1	–
SO_3, %	0.54	2.45	Portland cement at 7 days, % of control		
Na_2O, %	0.24	0.47	Strength activity index w/	85.5	–
K_2O, %	0.79	0.54	Portland cement at 28 days, % of control		
Total alkalies, %	0.76		Water required, % of control	94.6	–
Available alkalies, %	0.26	–			

Table 2
Mixture properties of ECC and mortar.

Ingredients	ECC-1 (M45)	ECC-2
Water (W), kg/m^3	331	327
Cement (PC), kg/m^3	570	386
Fly ash (FA), kg/m^3	684	847
Sand (S), kg/m^3	455	448
Fiber (PVA), kg/m^3	26	26
HRWR, kg/m^3	4.9	3.7
FA/PC	1.2	2.2
W/CM[a]	0.27	0.27
7-day compressive strength, MPa	38.1	21.6
28-day compressive strength, MPa	50.2	36.3
90-day compressive strength, MPa	55.4	41.9

[a] CM: cementitious materials (cement + fly ash).

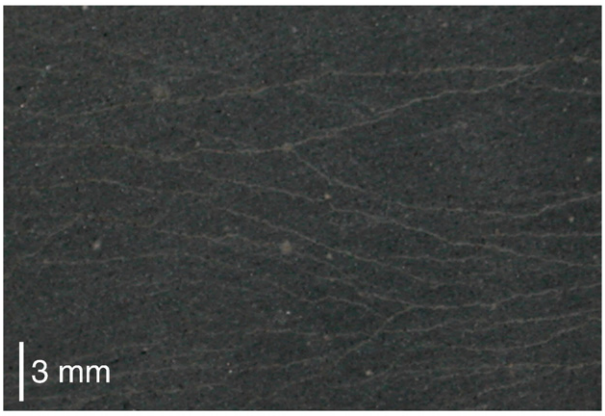

Fig. 2. Typical crack pattern on positive moment surface of ECC beams at 2 mm deformation [5].

AASHTO T259-80 (specimen surface shall be abraded if the concrete or treatment is to be subjected to the wearing effect of vehicular traffic (AASHTO T259)). Immediately after abrasion application, the prisms were pre-loaded using four-point bending test to obtain different crack widths. The ponding test was carried out with the pre-loaded specimens in the unloaded state. Some amount of crack closure occurred on unloading. To account for this, all crack width measurements were conducted in the unloaded stage. The widths of the crack were measured on the surface of the specimens along the span length (100 mm) by an optical microscope. The average width of the resulting crack was obtained through measurement of the crack widths at five points. Table 3 shows the pre-loaded beam deformation value, their corresponding average crack widths and number of cracks for prism specimens. Two virgin prisms from each mixture were tested without pre-loading for control purpose. Table 3 also shows the corresponding number of cracks for prism specimens at each beam deformation value. As seen from this table, when the deformation applied to the prism specimens is increased, the number of cracks on ECC is clearly increased but the crack width did not change for the different deformation values. Micro-mechanically designed ECC changes the cracking behavior from one crack with large crack width to multiple micro-cracks (Fig. 2).

After load application, plexiglass was used around the side surfaces of the prism to build an embankment for holding chloride solution on the exposed surface of prisms (Fig. 3). At 29 days of age, a 3% of NaCl solution was ponded on the cracked surface of prisms. In order to retard the evaporation of solution, aluminum plates were used to cover the top surface of the specimens. After 30 days of sodium chloride exposure, it was found that chloride penetration was concentrated at the locations of pre-cracks, and the penetration depth was deep, approximately 0–50 mm depending on the pre-loaded beam deformation value. For this reason, after 30 days of ponding, the salt solution was removed from the pre-loaded prism surface and powder samples were taken from each specimen for measuring chloride concentration with depth. For the virgin specimens, chloride concentration profile determination was conducted after 30 days and 90 days (in accordance with AASHTO T259-80) of NaCl solution exposure. In the case of the cracked ECC beams, chloride penetration occurs at multiple locations corresponding to where the multiple cracks were formed during the pre-load because, for cracked specimens, the majority of chloride penetration occurs through the crack and was not uniform through the material area. Fig. 3 also shows an irregular demarcation boundary (black profile) between the wet and dry zones revealed on the side-surface of the pre-cracked specimen after 30 days of NaCl solution exposure. For this reason, powder samples for chloride analysis of cracked ECC specimens were taken where the multiple cracks were formed during the pre-load (Fig. 3) by using a 15 mm diameter rotary drill bit. Total chloride content by weight of material at each sampling point was examined according to AASHTO T 260-97 [17].

The chloride profiles were then input into statistical and curve-fitting software. Crank's solution to Fick's second law, was fitted to the data (Eq. (1)) [18]. The regression analysis yielded the values of the effective diffusion coefficient (D_e) and surface chloride concentration (C_s) for each specimen.

$$C_{(x,t)} = C_s\left[1 - \left(\frac{x}{2\sqrt{D_e t}}\right)\right] \quad (1)$$

where, "x" is the distance from concrete surface; "t" is the exposure time; "$C_{(x,t)}$" is the chloride concentration at time "t" at depth "x"; "C_s" is the surface chloride concentration; "D_e" is the effective chloride diffusion coefficient; and "erf( )" is the error function. This equation assumes that concrete is homogenous in structure and that diffusion coefficient is independent of the moisture state of concrete, chloride concentration and temperature, and the binding isotherm is linear [19]. In reality, the transport behavior of the chloride ions in concrete is a more complex and complicated transport process than what can be described by Fick's second law of diffusion. For this reason, in this experimental study, the coefficient of diffusion found by regression analysis of chloride profiles using Eq. (1) is referred to as effective diffusion coefficient (D_e) that combined all transport mechanisms. Even though effective diffusion coefficient calculated from Eq. (1) is not a "true" diffusion coefficient, D_e forms a reasonable basis of

Table 3
Chloride ponding test — effective diffusion coefficient, crack widths and numbers of ECC prisms.

Mix ID	Beam deformation	Crack number[a]	Average crack widths	Diffusion coefficient		RCPT[b] coulomb
				m^2/s × 10^{-12}		
	mm		μm	30 days	90 days	
ECC-1 (M45)	0.0	0	–	6.7	4.6	501
	1.0	15	~50	28.0	–	–
	1.5	21	~50	37.5	–	–
	2.0	35	~50	54.2	–	–
ECC-2	0.0	0	–	10.7	5.1	1178
	1.0	6	~10	27.1	–	–
	1.5	26	~25	48.8	–	–
	2.0	36	~35	106.3	–	–

[a] Since all crack width measurements were conducted in the unloaded stage, the crack number, especially in the case of pre-cracked ECC-2 specimens, is likely undercounted due to the closing of many tiny cracks.

[b] Because of the expected differences in electrical resistance between two ECC mixtures, the RCPT values may reflect this difference and therefore should be interpreted with care.

Fig. 3. Typical ECC prisms (355×75×50 mm) during and after 30 days salt solution exposure and location of the sampling for chloride profiling.

comparing the transport properties of cracked and uncracked ECC specimens exposed to salt ponding.

The resistance to the chloride ion penetration of ECC mixtures was also measured by the Rapid Chloride Penetration Test (RCPT) at ages of 28 days in accordance with ASTM C1202 [20].

2.2.2. Sorptivity (absorption) test

At 28 days, all ECC beams (355×50×75 mm) were dried in an oven at 50±5 °C until a constant mass (constant mass — the difference between any two successive values is less than 0.5% of the lowest value obtained) is reached. The duration of the drying period to reach constant mass for ECC specimens was 3 days. Except for the control specimens, beam specimens were then pre-cracked by applying different deflections up to 2.0 mm using a four-point bending test to obtain different crack frequencies. After bending pre-load, 75×75×50 mm prisms from the central span of each beam specimen (100 mm) were cut for sorptivity tests. The sorptivity test was carried out with the pre-loaded oven dried ECC specimens in the unloaded state. As in the specimens for salt ponding test, all crack widths were measured in the unloaded state to account for crack closure on unloading. The number of cracks and crack width were measured using an optical microscope. The crack widths thus measured represent the maximum opening at the tensile surface of the beam. Table 4 shows the average crack widths, and corresponding number of cracks over the gauge length of 75 mm for the ECC prism specimens used for the sorptivity test. In the case of pre-cracked specimens, sorptivity value of ECCs is calculated from two oven dried specimens. For each mixture, three virgin (with no pre-loading) oven dried prisms were also tested for control purpose.

The sorptivity (absorption) test was based on ASTM C1585 [21]. The test consisted of registering the increase in mass of a prism specimen (75×75×50 mm) at given intervals of time (1, 2, 3, 4, 6, 8, 12, 16, 20, 25, 36, 49, 64, 81, 120 and 360 min) when permitted to absorb water by capillary suction. Only one surface of the specimen (negative moment surface — tensile face during pre-loading) was allowed to be in contact with water, with the depth of water between 3 and 5 mm (Fig. 4-a). A typical plot of the cumulative water absorption (normalized per unit surface area) as a function of the square root of time is shown in Fig. 4-b. It can be seen that the cumulative volume of water absorbed per unit surface area (mm^3/mm^2) in the specimens increased with the square root of time. This test was chosen as it measures the rate of ingress of water through unsaturated concrete. Therefore, it can be considered a measure of water transport associated with capillary suction.

2.2.3. Uniaxial tensile testing

ECC structural members may be exposed to high alkaline and/or marine environments (referred to as NaCl solution for this study) and alkalis and/or NaCl solution will penetrate through micro-cracks or even the uncracked matrix that could lead to modifications in the material microstructure and hence changes in the composite properties. Due to the delicate balance of cement matrix, fiber, and matrix/fiber interface properties, the strain capacity of ECC may change under high alkaline and marine exposure conditions. Therefore, the durability of composites (fiber plus matrix — ECC) must first be evaluated before it can be used in real field conditions.

After 28 days of curing, the coupon specimens were pre-loaded to 0.5, 1.0, 1.5 and 2.5% direct tensile strain to achieve various amounts of micro-cracking before exposure to sodium chloride (NaCl) solution, and to 1.0 and 2.0% direct tensile strain before exposure to sodium hydroxide solution (NaOH). Before testing, aluminum plates were glued to both ends of the coupon specimen to facilitate gripping. Tests were conducted on an MTS machine with 25 kN capacity under

Table 4
Sorptivity test — sorptivity, crack widths and numbers of ECC prisms.

ECC-1 (M45)				ECC-2			
Beam deformation (mm)	No. of cracks	Average crack widths (μm)	Sorptivity ($mm/min^{1/2}$)	Beam deformation (mm)	No. of cracks	Average crack widths (μm)	Sorptivity ($mm/min^{1/2}$)
0.0	–	–	0.028	0.0	–	–	0.030
0.5	2	~25	0.032	0.5	1	~10	0.032
0.5	3	~30	0.037	0.5	3	~15	0.039
0.5	4	~27	0.057	1.0	7	~17	0.075
1.0	5	~61	0.060	1.0	9	~20	0.088
1.0	6	~38	0.052	1.5	11	~19	0.099
1.0	7	~35	0.071	1.5	14	~18	0.114
1.5	9	~37	0.087	2.0	17	~23	0.165
2.0	14	~63	0.142	2.0	19	~17	0.187

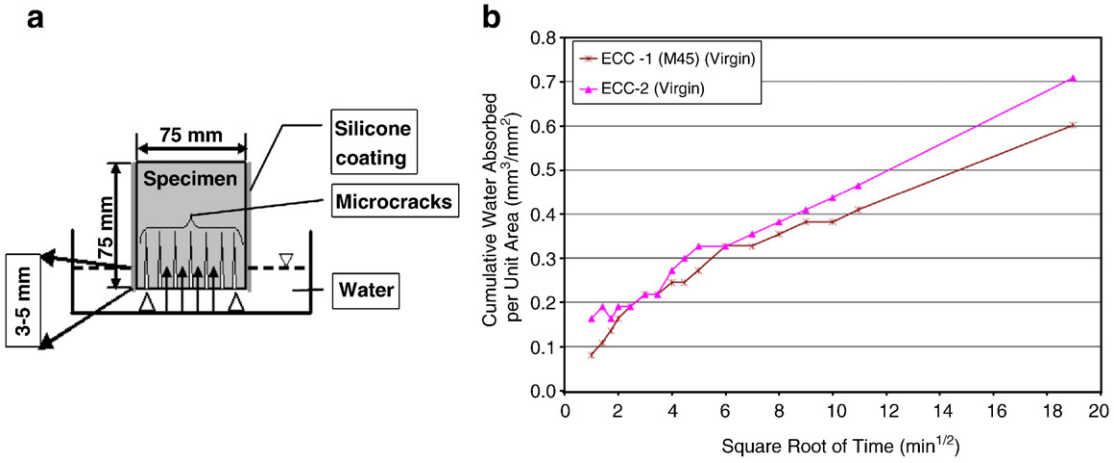

Fig. 4. (a) Schematic diagram of sorptivity test (specimen dimensions: 75×75×50 mm) [8], (b) typical result of water absorption as a function of square root of time.

displacement control at a rate of 0.005 mm/s. Typical stress–strain curves of the pre-loaded specimens are shown in Fig. 5.

When the tensile strain reached the required pre-determined strain value, the tensile load was released. As in the beam specimens after bending test, a small amount of crack closure occurred on unloading. To account for this, all crack widths were measured in the unloaded stage. The widths of the crack were measured on the surface of the specimens with an optical microscope. Table 5 shows the pre-loading tensile strain value, their corresponding average crack widths, and number of cracks within the pre-cracked coupon specimens. The gage length used in these measurements was about 50 mm. As seen from Table 5, even at large uniaxial tensile strain level, crack widths of ECC remain nearly constant, while the number of cracks on tensile surface of the ECC specimens increased. As expected, a higher tensile strain coincides with more cracks. Fig. 5 also shows typical stress–strain curves of ECC specimens that had been pre-cracked to 1% or 2% strain levels, then unloaded, and immediately reloaded. Thus, these specimens had no time to undergo any crack healing. As expected, there is a remarkable difference in initial stiffness between virgin specimen and pre-cracked specimen under direct tension. This is due to re-opening of cracks within pre-cracked specimens during re-loading [22]. The opening of these cracks offers very little resistance to load, as the crack simply opens to its previous crack width before fiber bridging is fully re-engaged. Once fiber bridging is re-engaged, however, the load capacity resumes, and further tensile straining of the intact material can take place.

The pre-loaded ECC specimens together with some uncracked (virgin) specimens without pre-loading were then continuously immersed in 1 N NaOH solution at 38 °C for 30 and 90 days, and 3% NaCl solution at room temperature for 30, 60, 90 and 180 days. Subsequently direct tensile measurements on these specimens were conducted and stress–strain curves were recorded. In the case of uncracked specimens, average strain capacity, ultimate strength and residual crack width of ECC are an average of four specimens. In the case of pre-cracked specimens, average strain capacity, ultimate strength and residual crack width of ECC are calculated from a minimum of four and maximum of six specimens. For control purpose, virgin specimens were also tested up to 180 days of additional curing (after 28 days) in laboratory condition (50±5% RH, 23±2 °C).

3. Results and discussions

3.1. Salt ponding and rapid chloride permeability tests (RCPT)

The chloride concentration profiles of uncracked and cracked ECC specimens from the ponding test of prism specimens are shown in Fig. 6. The chloride contents at different depths from the exposed surface were determined after 30 days of exposure to chloride environment. As in the virgin specimens (beam deformation — BD=0), the chloride content in the micro-cracked zone decreased with increasing depth because micro-cracks generated in beams under bending load had a crack width reducing along its depth (V-shaped). As seen from Fig. 6, the multiple cracking in ECC due to pre-loading alters the transport properties measured as a function of beam deformation.

The effective chloride diffusion coefficients of prisms, calculated in accordance with Fick's second law, are summarized in Table 3. The

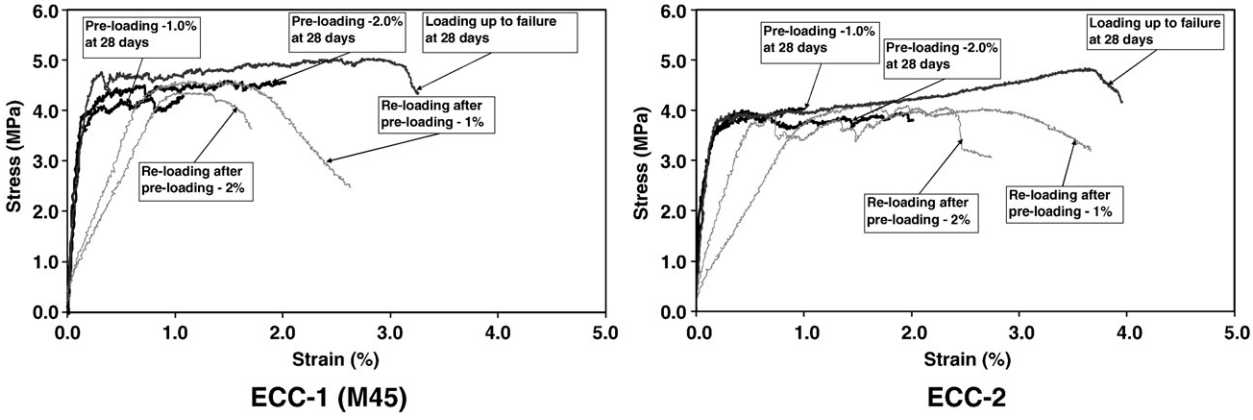

Fig. 5. A typical tensile stress–strain curves for pre-loading and re-loading ECC specimens.

Table 5
Crack widths and numbers of pre-cracked ECC coupons.

ECC-1 (M45)			ECC-2		
Pre-loading tensile strain (%)	Average crack widths (μm)	Crack number	Pre-loading tensile strain (%)	Average crack widths (μm)	Crack number
0.5	~36	7	0.5	~24	7
1.0	~44	12	1.0	~30	16
1.5	~50	16	1.5	~28	23
2.0	~55	21	2.0	~38	25
–	–	–	2.5	~31	37

effective diffusion coefficients of the virgin ECC specimens calculated on the basis of 30 days of exposure are higher than that of 90 days of exposure. This exposure age dependence of effective diffusion coefficient is due to the continuing PC&FA hydration process which is beneficial in reducing pore sizes and densifying the matrix [23]. Table 3 also shows the relationship between the effective diffusion coefficient and beam deformation level/crack width–number in ECC specimens exposed to NaCl solution for 30 days. As seen from Table 3, the crack width of all specimens even at large imposed deformation level is lower than 50 μm, while the number of cracks on tensile surface of the ECC specimens increased. Fig. 7 shows the relationship between the effective diffusion coefficient of chloride ions and the beam deformation level for ECC specimens exposed to NaCl solution for 30 days. As seen from the figure, the effective diffusion coefficients of ECC-1 increase at a steady rate with the imposed deformation value (or number of cracks), which is in agreement with research findings by Konin et al. [24]. On the other hand, for the higher deformation level (BD > 1 mm), the effective diffusion coefficients of ECC-2 increase suddenly at higher deformation levels. It is speculated that this sudden increase in effective diffusion coefficient of ECC-2 is associated with the increase in the number of extremely tiny cracks, which were not detected due to their closing on specimen unloading. Since the micro-cracked specimens are almost dry when they are first exposed to salt solution in accordance with AASHTO T259, the presence of even almost closed tiny cracks may affect the chloride penetration significantly because of capillary suction (see Section 3.2). In addition to crack number and width, crack length may also influence the effective diffusion coefficient of ECC. However, due to the tight crack width, it is not easy to quantify the cracks length accurately in micro-cracked ECC. Further studies are needed to properly quantify the crack width and crack depth of micro-cracked ECC, and their effects on effective chloride diffusion of ECC.

For comparison purpose, typical values for the effective diffusion coefficient found in the literature are given in Table 6. It should be noted that values of effective diffusion coefficient found in the literature are generally determined by different methods, maturity and curing conditions, and the resulting values are influenced by the methodology employed. As seen (Tables 3 and 6), the effective chloride diffusion coefficient of virgin ECC is not significantly different than that of normal mortar or concrete determined from previously investigations. Moreover, both ECC materials revealed a significantly smaller effective diffusion coefficient compared to the mortar specimens pre-loaded to the same deformation level (Fig. 7), reflecting the reduction in chloride ion transport rate as a result of tight crack width control in the ECC [5], which is also in agreement with research findings by Ismail et al. [27].

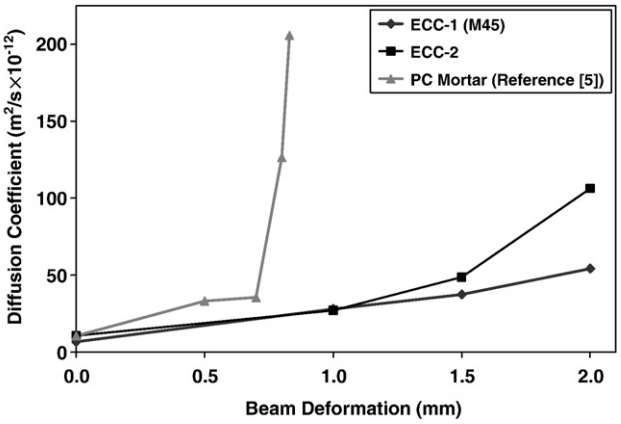

Fig. 7. Effective diffusion coefficient (calculated after 30 days of sodium chloride exposure) versus pre-loading beam deformation level.

The reason for the relatively low effective diffusion coefficient of cracked ECC specimens is not only due to the tight crack width but also the presence of self-healing of the micro-cracks. Based on experimental results, Şahmaran et al. proposed that micro-cracks of ECC can be easily closed by a self-healing process even after exposure for 30 days to NaCl solution [5]. The results of a study conducted by Ismail et al. also confirm that in the case of cracks with width below 60 μm, the self-healing potential of the mortar matrix can impede the effective chloride diffusion along a crack path [27]. The observed self-healing in ECC can be attributed primarily to the large FA content and relatively low water to binder ratio within the ECC mixture [4–6,9,11]. The continued pozzolanic activity of unhydrated FA and cement particles is responsible for the self-healing of the crack which reduces the ingress of the chloride ions [4–6,9,11].

Cracks opened to a maximum width of approximately 50 μm within the ECC-1 specimens, and 35 μm within the ECC-2 specimens. However, as seen from Table 3 and Fig. 7, no significant difference in

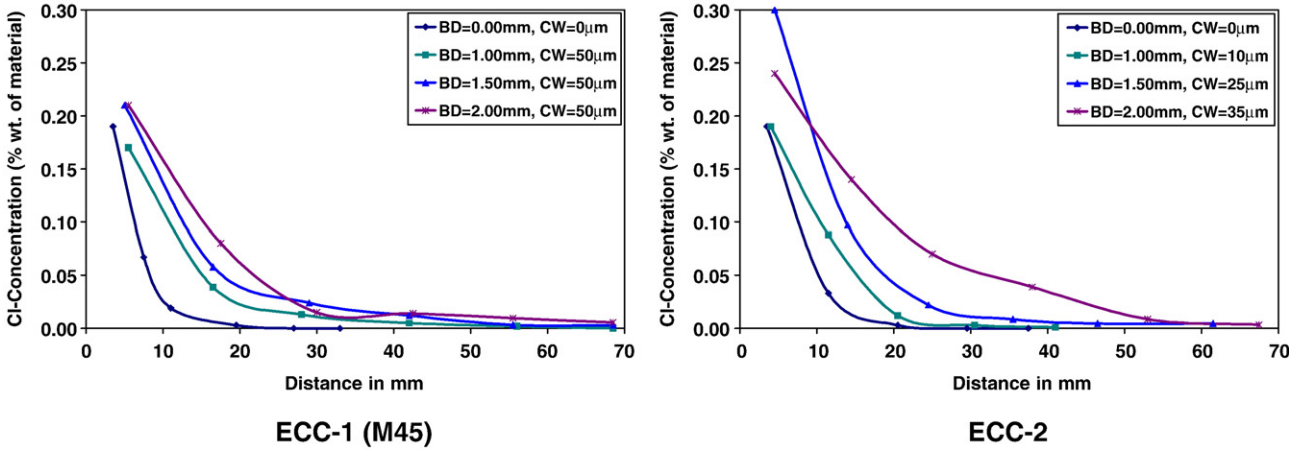

Fig. 6. Chloride profiles of ECC prisms in cracked zone at 30 days exposure.

Table 6
Typical values for the effective chloride diffusion coefficient.

Source	Material	W/CM	Paste vol. (%)	Diffusion coefficient ($m^2/s \times 10^{-12}$)
Page et al. [25][a]	PC paste	0.50	100	4.50
	PC paste + 30% FA	0.50	100	1.50
	PC paste + 65% GBFS	0.50	100	0.40
McGrath and Hooton [26][b]	PC concrete	0.40	35	6.30
	PC + 8% GBFS concrete	0.40	35	2.25
	PC + 8% FA concrete	0.40	35	3.35
	PC + 8% SF concrete	0.40	35	0.88
	PC + 40% GBFS + 8% SF concrete	0.31	40	0.21
	PC + 30% FA + 8% SF concrete	0.31	40	0.30
Şahmaran et al. [5][c]	PC mortar (BD = 0.00 mm–CW = 0 μm)	0.35	40	10.58
	PC mortar (BD = 0.50 mm–CW = 50 μm)	0.35	40	33.28
	PC mortar (BD = 0.70 mm–CW = 150 μm)	0.35	40	35.54
	PC mortar (BD = 0.80 mm–CW = 300 μm)	0.35	40	126.53
	PC mortar (BD = 0.83 mm–CW = 400 μm)	0.35	40	205.76

[a] Diffusion coefficients were calculated after 60-day moist curing at 22 °C.
[b] Diffusion coefficients were calculated after 56 days moist at 23 °C.
[c] Diffusion coefficients were calculated after specimens were subjected to the same curing condition and period as applied in this study.

the effective diffusion coefficient was observed when crack widths were changed between the 10 and 50 μm (The data point for beam deformation of 2.00 mm actually shows an increase of effective diffusion coefficient with a decrease of crack width from 50 μm (ECC-1) to 35 μm (ECC-2.)). Therefore, distinct from the mortar specimens that showed significant increase in effective diffusion coefficient when the crack width increases, especially at larger than 150 μm [5], the effective diffusion coefficient appears not to follow this trend for ECC specimens. Moreover, even though ECC-2 (FA/PC = 2.2) has tighter crack width compared with ECC-1 (FA/PC = 1.2) specimens, the effective diffusion coefficients of ECC-2 for the virgin and micro-cracked specimens are higher than that of ECC-1 specimens, at given beam deformations. Normally, it is accepted that increasing FA content is an effective means for reducing the coefficient of effective chloride diffusion due to both its chloride binding effect and pore refinement [28]. These benefits, however, are usually manifested at later ages with little improvement being observed after ages of 28 days or so [29].

The rapid chloride permeability test results for virgin ECC mixtures at 28 days are also shown in Table 3. They are expressed in terms of the total electrical charge in coulombs, which provides an indirect measure of the resistance of ECC to chloride ion penetration. The data presented in Table 3 show that standard ECC mixture (ECC-1 (M45)) exhibited excellent resistance to chloride ion penetration with the total charge exceeding 501 C at the age of 28 days. On the other hand, increasing FA content from 55% to about 70% reduces the resistance to chloride ion penetration of ECC. This trend is in stark contrast to that observed from previous studies; HVFA (up to 70%) can considerably improve the performance of concrete in terms of reduced chloride ion penetration according to ASTM C1202 test method [30]. The reason for the observed lower resistance to chloride ion penetration in the case of ECC-2 may be attributed to the fact that specimens were cured in air after a 7-day sealed curing, and because of lack of curing, most of the FA particles in the matrix remain without any chemical reaction. Since ECC-2 has more FA content than ECC-1, it has been more negatively affected by the lack of curing. The benefits of using Class-F FA in concrete in terms of improved durability properties such as chloride ion penetration resistance is usually manifested at later ages with the continuous supply of moisture [30].

In spite of the increase in RCPT value, the ECC-2 still satisfies a low chloride ion penetration level, according to ASTM C1202. It should also be noted that the RCPT results depend on the electrical conductivity of pore solution, which is determined by the composition of the pore solution. The electrical conductivity or RCPT value of a concrete can be reduced by lowering the alkalinity of concrete pore solution. When FA with low lime and low alkali contents, as in this study (Table 1), is used to partially replace PC, the concentration of alkali ions and associated hydroxyl ions in the pore solution generally decreases significantly, and the extent of this reduction depends also on FA replacement level [31]. Because of the expected differences in electrical resistance between two ECC mixtures, however, the electrical conductivity values may also be different. As a result, the RCPT values may reflect this difference and therefore should be interpreted with care.

3.2. Sorptivity test

Table 4 presents the sorptivity values of the ECC mixtures determined after a 28-day curing period. Sorptivity test was conducted to determine how load-induced micro-cracks of ECC affect the capillary suction (absorption) of concrete. The cumulative water absorption per unit area of the specimen up to 6 h was fitted using linear regression and the equation obtained was used to describe capillary actions in the first 6 h. Fig. 8 shows the relationship between the sorptivity ($mm/min^{1/2}$) over 6 h and the number of cracks, for ECC specimens. Corresponding values for virgin ECC specimens (data points with zero number of cracks) are also included in this plot. As seen from the figure, the presence of micro-cracking in ECC significantly alters the transport properties measured as a function of the number of micro-cracks. The water absorption increase is fairly high as the number of cracks on the surface of the ECC specimens increases. Therefore, the sorptivity test shows that micro-cracked ECC specimens would be more vulnerable to attack than virgin specimens. As the number of cracks along the specimen grows, the sorptivity of ECC increased exponentially. From Fig. 8, the effect of increasing FA content from 55% to about 70% on the sorptivity values could not be discerned. It should be noted that because of the closing of many tiny cracks in the unloaded stages, the crack number, especially in the case of the pre-cracked ECC-2 specimens, is likely undercounted. As a result, the correlation between the crack density and sorptivity value may be different, and therefore should be interpreted with care.

According to Neville [32], typical sorptivity is 0.09 $mm/min^{1/2}$ for oven dried at 105 °C normal concrete specimen with a W/C ratio of 0.40. Other research suggested that ordinary Portland cement concrete with W/C ratio of 0.40–0.50 would have sorptivity of about 0.23 $mm/min^{1/2}$ [33–35]. Therefore, the measured sorptivity (<0.19 $mm/min^{1/2}$) for the cracked ECC specimens was not particularly high when compared to that of conventional concrete. The reason for the lower sorptivity of ECC mixtures may be attributed to a

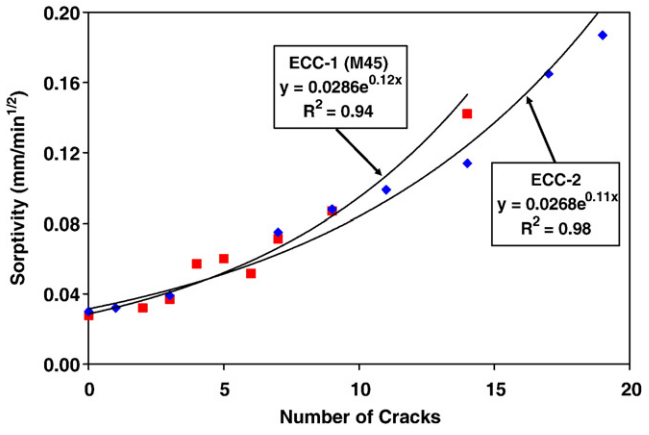

Fig. 8. Sorptivity versus number of crack.

significantly lower W/CM ratio, high FA content and absence of coarse aggregate. The use of FA probably resulted in a denser matrix, by reducing the pore size and thickness of transition zone between fiber and surrounding cementitious matrix [36]. According to the Mehta and Monteiro [37], the existence of micro-cracks in the interfacial transition zone at the interface with coarse aggregate is the primary reason that concrete is more permeable than the corresponding hydrated cement paste and mortar. Moreover, Şahmaran and Li [8] also studied the absorption rate in cracked ECC, and found that the use of water repellent admixture in the production of ECC could easily inhibit the sorptivity even for the mechanically pre-loaded ECC.

Moreover, the sorptivity values of cracked ECC specimens given in Table 4 likely represent upper limits of sorptivity in actual structures. This is because the effect of self-healing of micro-cracked ECC has not been accounted for in these specimens due to the short experimental duration. In this experimental study, the sorptivity of ECC specimens was determined following exposure to water for 6 h. Under wet and dry cycles, micro-cracks in ECC were found to close due to self-healing [5,22], thus slowing further water intake and reducing the rate of water absorption. As also mentioned above, this healing can be due to continued hydration of unhydrated particles in the composites, creating C–S–H bridges between crack lips. Even though the adding FA from 55% (FA/PC = 1.2) to about 70% (FA/PC = 2.2) on sorptivity value appeared to be insignificant, the use of HVFA–ECC are likely to promote self-healing behavior since the crack width reduces as FA content increases at all ages (see crack widths in Tables 3, 4 and 7).

3.3. Uniaxial tensile behavior

3.3.1. Under laboratory environment

Table 7 shows the tensile behavior of ECC mixtures cured in air at different ages, after an initial 7-day moist curing. These ECC composites exhibited a strain capacity of more than 3.5% at 7 days. The strain capacity measured after 7 days is lower than the 7-day strain capacity for both ECC mixtures; however the observed ~3.0% long-term strain capacity remains acceptable for an ECC. This slight drop in long-term strain capacity should be accounted for by using the lower long-term value in structural design. Based on the similarity of test results up to 210 days, the tensile strain capacity seems to stabilize at about 3.0% for ECC-1 (M45) and 3.5% for ECC-2 after 28 days. The time dependent strain capacity change described above has been known for sometime and is ascribed to the increase in fiber/matrix interface properties and matrix toughness associated with the continued PC&FA hydration process [14]. As can be seen from Table 7, the increase of FA–PC ratio improves the tensile strain of ECC at all ages. The improvement in the tensile strain with the increase in the FA content can be attributed to the fact that increase in the FA content tends to reduce the PVA fiber/matrix interface chemical bond and matrix toughness, while increasing the interface frictional bond, in favor of attaining high tensile strain capacity [14]. On the other hand, the increase in the FA content did not influence the tensile strength, and it is above 4.0 MPa at all ages except for ECC-2 at 7 days. Table 7 also gives the effect of FA content on the residual crack width at different ages. It was found that the crack width reduces significantly as FA content increases at all ages. At the age of 210 days, the residual crack width of ECC-2 is about 10 μm. The reason for this is not completely clear, but is likely associated with the higher fiber/matrix interface frictional bond. The lower magnitude of the crack width is expected to promote the self-healing behavior, and thus the transport properties in cracked composites, and aids in enhancing structural durability.

3.3.2. Under high alkali exposure

Even though no deleterious expansion has been expected due to alkali silica reaction because of the high volume FA content, small sand particle size and micro-fibers in ECC [6], durability of HVFA–ECC must be evaluated under high alkaline environments. Alkalis will penetrate through micro-cracks or even the uncracked matrix that could lead to modifications in the material microstructure and hence changes in the composite properties. Table 8 summarized the tensile strain capacity, tensile strength, and crack width of ECC with various pre-loaded strain values, and alkali exposure condition at 38 °C. Typical tensile stress–strain curves obtained for coupon specimens pre-cracked at 28 days and subsequently immersed in an alkali solution, and control specimens cured in air are shown in Fig. 9. As seen in this figure, the first-cracking strength of pre-cracked ECC specimens after alkaline solution immersion falls below the first-cracking strength of the virgin specimens cured in air and in alkaline environment. By comparing the initial material stiffness of reloaded ECC specimens stored in sodium hydroxide solution in Fig. 9 with that shown for the reloaded specimens before exposure in Fig. 5, it can be observed that a significant recovery of mechanical stiffness has been achieved. This suggests that between the time of inducing pre-cracking and the time of testing, after immersion in alkaline solution, healing of the micro-cracks has occurred in the ECC specimens. This can be attributed primarily to the high CM content and relatively low W/CM ratio within the ECC mixture. As a result of the formation of micro-cracks due to mechanical loading, unhydrated cementitious particles are easily exposed to the NaOH solution at 38 °C, which leads to the development of further hydration processes. Finally micro-cracks under conditions of a wet environment were closed by newly formed products. Newly formed C–S–H gels in the micro-cracks of ECC specimens subjected to NaOH solution are also evident from the ESEM observations [6].

The average ultimate tensile strength and strain values are summarized in Table 8. Compared to control specimens cured in laboratory air, the test results indicate that the ECC specimens stored

Table 7
Tensile properties of ECC specimens cured in laboratory air after 7-day moist curing.

Specimen type		Tensile strain (%)	Tensile strength (MPa)	Residual crack width (μm)
ECC-1 (M45)	7 d.	3.90 [0.65]	4.46 [0.15]	~56
	28 d.	2.70 [0.63]	4.96 [0.40]	~51
	60 d.	2.86 [0.58]	4.81 [0.64]	~45
	90 d.	2.51 [0.19]	4.75 [0.32]	~35
	120 d.	3.02 [0.60]	4.64 [0.32]	~28
	210 d.	2.83 [0.40]	4.39 [0.17]	~26
ECC-2	7 d.	4.54 [0.26]	3.32 [0.20]	~37
	28 d.	3.51 [0.08]	4.35 [0.46]	~28
	60 d.	4.18 [0.55]	4.15 [0.42]	~23
	90 d.	3.65 [0.60]	4.31 [0.20]	~18
	120 d.	3.34 [0.20]	4.22 [0.28]	~10
	210 d.	3.82 [0.48]	4.33 [0.33]	~10

Numbers in brackets are standard deviations.

Table 8
Tensile properties of ECC under alkali exposure conditions.

Specimen type		Tensile strain (%)	Tensile strength (MPa)	Residual crack width (μm)
ECC-1 (M45)	Pre-loading—0.0%, 30 d.	2.80 [0.23]	4.64 [0.67]	~85
	Pre-loading—0.0%, 90 d.	2.49 [0.56]	4.55 [0.17]	~85
	Pre-loading—1.0%, 30 d.	2.73 [0.37]	4.36 [0.19]	~75
	Pre-loading—1.0%, 90 d.	2.51 [0.21]	4.56 [0.46]	~80
	Pre-loading—2.0%, 30 d.	2.75 [0.41]	4.21 [0.13]	~95
	Pre-loading—2.0%, 90 d.	2.44 [0.38]	4.39 [0.45]	~90
ECC-2	Pre-loading—0.0%, 30 d.	2.79 [0.21]	4.52 [0.33]	~65
	Pre-loading—0.0%, 90 d.	2.52 [0.16]	4.46 [0.18]	~55
	Pre-loading—1.0%, 30 d.	2.62 [0.28]	4.32 [0.56]	~65
	Pre-loading—1.0%, 90 d.	2.26 [0.21]	4.40 [0.11]	~50
	Pre-loading—2.0%, 30 d.	2.70 [0.56]	4.23 [0.32]	~65
	Pre-loading—2.0%, 90 d.	2.07 [0.07]	4.25 [0.23]	~65

Numbers in brackets are standard deviations.

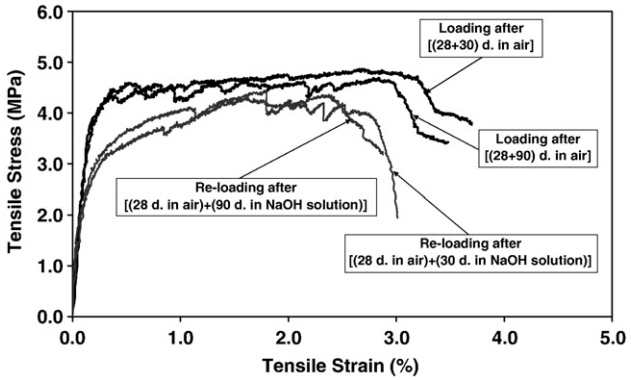

Fig. 9. Effect of alkali exposure on tensile behavior of ECC-1 (M45) specimens pre-loading to 2% tensile strain [6].

in NaOH solution show a slightly lower or similar ultimate tensile strength, and lower tensile strain values with the specimens cured in laboratory air. However, the tensile strain capacity given in this table does not include the residual strain from the pre-cracking load as explained in Section 2.2.3 (Uniaxial tensile testing). By neglecting this residual strain, the large variability in material relaxation during unloading is avoided, and a conservative estimation for ultimate strain capacity of the material is presented. The tensile strain capacity of virgin and pre-cracked ECC specimens exposed to NaOH solution averaged between 2.44% and 2.80% for ECC-1 (M45) and 2.07% and 2.79% for ECC-2. Increasing levels of FA lead to higher reductions in the tensile strain capacity compared with standard ECC mixture (ECC-1, M45).

The reduction in tensile strain capacity of ECC specimens stored in NaOH solution at 38 °C may be attributed to changes of the fiber/matrix interface. For example, Li et al. [12] examined the interfacial microstructure change of PVA–ECC in hot water (60 °C) exposure. They observed that after immersing the composite in hot water for 26 weeks, the fiber bridging property has deteriorated through an increase in the chemical bond (G_d) of the fiber–matrix interface combined with a decrease in the apparent fiber strength (σ_{fu}^{APP}). This combination of changes in G_d and σ_{fu}^{APP} results in a crack bridging stress-crack opening curve that has smaller complementary energy than the same ECC without hot water exposure. Consequently, the condition for strain hardening is more readily violated in such composites after long-term exposure, leading to unsaturated multiple cracking and associated reduced strain capacity [12]. In the case of higher FA content (ECC-2), alkalis may more easily penetrate through matrix because of lower matrix strength and compactness especially at early ages, and that could lead to more modifications in the material microstructure and hence changes in the composite properties. Despite a reduction in ductility, both of the ECC mixtures after 90 days of alkali solution exposure are found to retain tensile ductility at least more than 200 times that of normal concrete and FRC with no environmental exposure. For this reason, it is expected that the ECC composites investigated are suitable for long-term application under high alkaline environments if the structure is designed based on long-term mechanical properties. Moreover, exposure condition used in this study provides a continuous supply of alkali ions. Such a supply may not be available in real field conditions and therefore, the present test may impose a more accelerated and severe exposure environment when compared with real field conditions.

The residual crack width at different ages of ECC mixtures are also given in Table 8. The term residual crack width of ECC indicates that crack width was measured from the unloaded specimen after the direct tensile test. The residual crack width of virgin and pre-cracked specimens exposed to NaOH solution is wider than that of sound air cured specimens, but remains less than 100 μm. In terms of permeability and diffusion, crack width less than 100 μm generally behave like sound concrete [5,11]. Based on previous experimental results [4–6,9,22], the authors proposed that cracks with width below 100 μm can experience self-healing. However, more experimental studies on a micro-mechanical scale are necessary to clearly understand the mechanisms behind the reduction in the ultimate tensile strain, strength and increased crack width.

3.3.3. Under sodium chloride exposure

Table 9 summarized the tensile strain, strength, and crack width of ECC specimens with various pre-loaded strain value and NaCl solution exposure conditions. Typical tensile stress–strain curves obtained for specimens before and after exposure to NaCl solution are shown in Fig. 10. By comparing the initial material stiffness of reloaded ECC specimens exposed to NaCl solution, as in the exposure of NaOH solution, it can be observed that a significant recovery of elastic stiffness has been achieved. This suggests that between the time of inducing pre-cracking and the time of testing, after exposure to NaCl solution, healing of the micro-cracks has also occurred in the ECC specimens. The reason of self-healing has already been discussed before and in Refs. [5] and [9].

The average ultimate tensile strength values are shown in Table 9. Compared to control specimens cured in laboratory air (Table 7), despite some scattering in the test results, the specimens (pre-cracked and uncracked) stored in NaCl solution show a slight reduction in ultimate tensile strength over the 180-day exposure period; this may be attributed to the effects of damage on the fiber/matrix interface due to immersion of humid environment [12,14]. The other reason of slight reduction in the tensile strength of ECC specimens when exposed to NaCl solution may be attributed to the effects of leaching of calcium hydroxide from the specimens [9]. Water not saturated with calcium hydroxide (high-calcium hydrated lime) may affect test results due to leaching of lime from the test specimens [38]. However, more experimental studies on a micro-mechanical scale are necessary to understand the reasons of the reduction in the ultimate tensile strength.

Table 9 also summarizes the average of tensile strain capacity of ECC specimens stored in NaCl solution. The tensile strain capacity reported for these specimens also does not include the residual strain from the pre-cracking load. As seen from the table, for the uncracked

Table 9
Tensile properties of ECC under different NaCl exposure conditions.

Specimen type		Tensile strain (%)	Tensile strength (MPa)	Residual crack width (μm)
ECC-1 (M45)	Pre-loading—0.0%, 30 d.	2.79 [0.54]	4.34 [0.62]	~100
	Pre-loading—0.0%, 90 d.	3.27 [0.76]	4.41 [0.45]	~100
	Pre-loading—0.0%, 180 d.	2.48 [0.28]	4.27 [0.32]	~100
	Pre-loading—0.5%, 30 d.	3.85 [0.61]	4.59 [0.29]	~100
	Pre-loading—0.5%, 90 d.	3.22 [0.39]	4.70 [0.35]	~100
	Pre-loading—0.5%, 180 d.	2.62 [0.30]	4.41 [0.48]	~100
	Pre-loading—1.0%, 30 d.	2.66 [0.66]	3.85 [0.09]	~100
	Pre-loading—1.0%, 90 d.	2.61 [0.12]	4.12 [0.17]	~100
	Pre-loading—1.0%, 180 d.	2.09 [0.19]	4.38 [0.89]	~100
	Pre-loading—1.5%, 30 d.	2.48 [0.94]	3.87 [0.73]	~100
	Pre-loading—1.5%, 90 d.	2.96 [0.87]	4.17 [0.17]	~100
	Pre-loading—1.5%, 180 d.	1.91 [0.20]	3.94 [0.01]	~100
ECC-2	Pre-loading—0.0%, 30 d.	4.09 [0.54]	3.81 [0.46]	~70
	Pre-loading—0.0%, 90 d.	3.23 [0.25]	4.07 [0.61]	~70
	Pre-loading—0.0%, 180 d.	2.75 [0.87]	4.45 [0.47]	~70
	Pre-loading—0.5%, 30 d.	3.56 [0.56]	3.69 [0.32]	~70
	Pre-loading—0.5%, 90 d.	3.00 [0.36]	3.72 [0.29]	~70
	Pre-loading—0.5%, 180 d.	2.68 [0.50]	4.39 [0.49]	~70
	Pre-loading—1.5%, 30 d.	3.67 [1.13]	3.91 [0.78]	~70
	Pre-loading—1.5%, 90 d.	2.93 [0.34]	3.65 [0.20]	~70
	Pre-loading—1.5%, 180 d.	2.29 [0.30]	3.87 [0.23]	~70
	Pre-loading—2.5%, 30 d.	3.47 [0.57]	3.76 [0.52]	~70
	Pre-loading—2.5%, 90 d.	2.78 [0.30]	3.90 [0.09]	~70
	Pre-loading—2.5%, 180 d.	2.32 [0.64]	3.84 [0.27]	~70

Numbers in brackets are standard deviations.

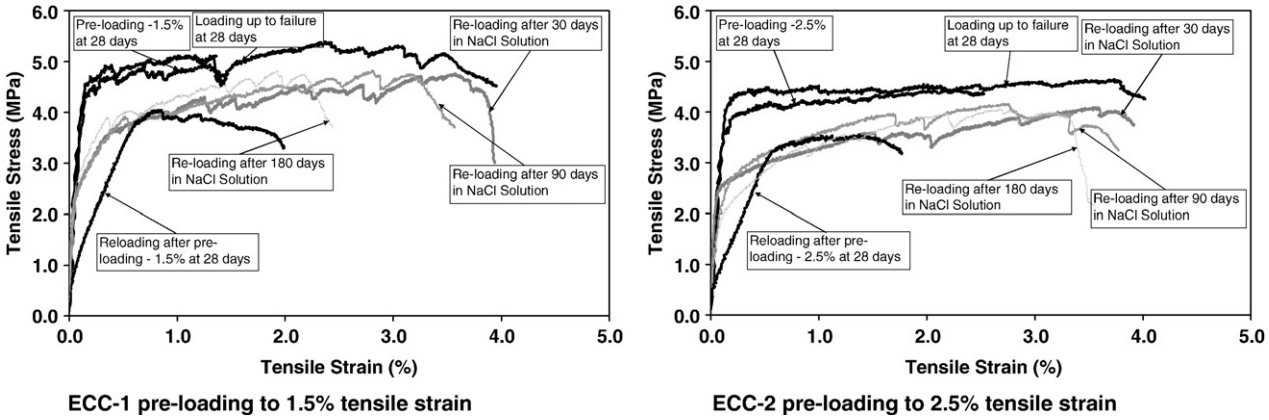

Fig. 10. Typical tensile stress–tensile strain curves of micro-cracked ECC specimens before and after exposed to 3% NaCl solution.

specimens, the tensile strain capacity does not appear to be affected up to 90-day exposure period. For the pre-cracked specimens, exposure to NaCl appears to be similarly affected, such that the influence of pre-cracking even up to 1.5% for ECC-1 and 2.5% for ECC-2 does not exacerbate the deterioration. However, after 180-day NaCl solution exposure period, both uncracked and cracked specimens showed a reduction of up to 30% in their tensile strain capacity, but their tensile strain capacity is still higher than 2%. Both of the ECC mixtures showed also almost the same percentage of reductions in terms of tensile properties, and therefore, the increase in the FA content did not change the behavior of ECC specimens exposed to continuous NaCl solution. Table 9 also shows the residual crack width of ECC mixtures at different ages. As in the ECC specimens exposed to NaOH solution, the residual crack width of virgin and pre-cracked specimens exposed to continuous NaCl solution is wider than that of virgin air cured specimens, but remains less than 100 μm for both of the ECC mixtures.

In the case of pre-cracked specimens exposed to NaCl solution, a distinct white deposit was visible, which formed a continuous dense layer over the crack surface (Fig. 11). The deposits were most probably caused by efflorescence due to the leaching of calcium hydroxide into cracks [9]. It has also been suggested that in marine environment this effect may arrest chloride transportation by healing of cracks. From the present study, healing of micro-cracks of both ECC mixtures under NaCl solution is evident from the mechanical properties discussed before. The mechanical properties indicate that micro-cracks of ECC exposed to NaCl solution healed almost completely.

4. Conclusions

The results of experiments monitoring the change in the transport and tensile properties of ECC materials subjected to mechanical pre-loading and accelerated aging are presented in this paper. The magnitude of beam deformation level is found to have deleterious effect on the effective chloride diffusion coefficient and sorptivity values. Even though ECC-2 (FA/PC = 2.2) specimens after mechanical pre-loading has tighter crack width compared with ECC-1 (FA/PC = 1.2) specimens, the transportation values, especially effective diffusion coefficients of ECC-2 for the virgin and micro-cracked specimens, at the same beam deformation level are higher than that of ECC-1 specimens.

Specimens exposed to a continuous NaCl solution at room temperature or NaOH solution at 38 °C generally show decreases in tensile strain capacity and slight decrease or no change in tensile strength compared with the specimens cured in air. Furthermore, the crack width increases to around 1.5 times or above compared with that of air curing specimens. This phenomenon suggests possible change in the fiber/matrix interface bond properties after accelerated

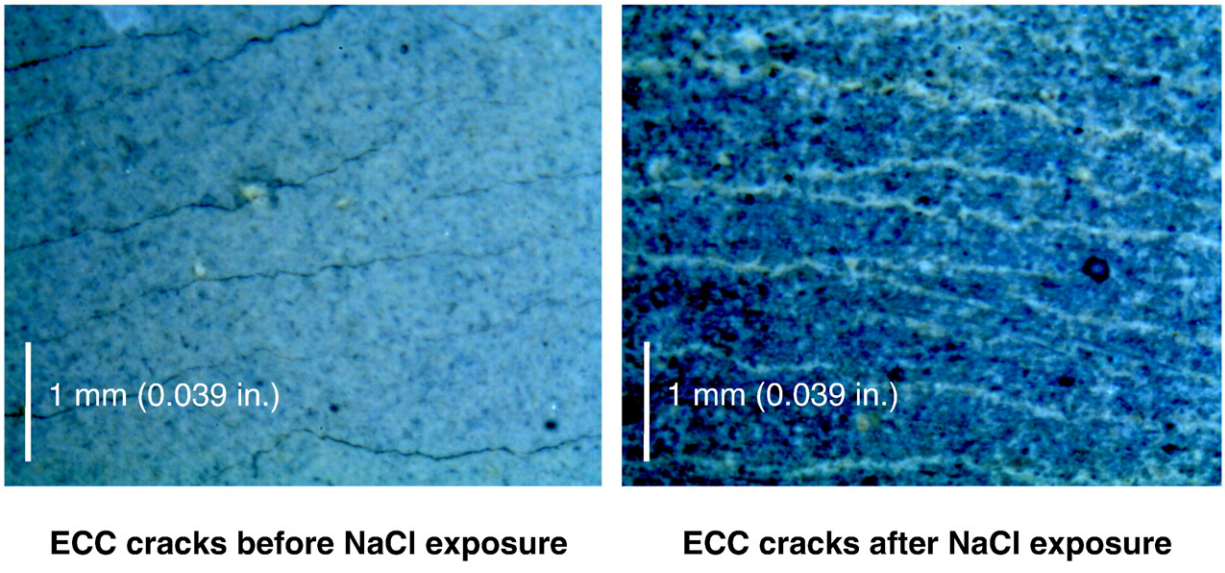

Fig. 11. Self-healing products in ECC micro-cracks before and after exposed to 3% NaCl solution.

aging. Apart from the slight reductions in ultimate tensile strain and strength capacities and higher residual crack width, the results presented in this study largely confirm the durability performance of ECC material in terms of mechanical properties under accelerated aging (exposure to continuous sodium hydroxide at 38 °C and sodium chloride solutions at room temperature), even in cases where the material experiences mechanical loading that deforms it into the strain-hardening stage prior to exposure. Healing of micro-cracks induced by the pre-load is evident from the recovery of elastic stiffness of the exposed pre-cracked specimens on re-loading. Moreover, the mechanical performance of ECC after accelerated aging is not significantly influenced by the FA content.

It may be possible to further extend FA volumes in ECC. Previously performed investigations have indicated that increasing levels of FA leads to improvements in tensile properties and reductions in crack width compared with standard ECC mixture (M45). However, there is likely to be an upper limit, beyond which compressive strength of HVFA–ECC cannot reasonably match that of structural concrete, and there is no further benefit with respect to its durability properties as discussed in this study.

Acknowledgments

The first author would like to acknowledge the financial support of TUBITAK (The Scientific and Technical Research Council of Turkey) provided under Project: MAG-108M495. This research was partially funded through an NSF MUSES Biocomplexity Program Grant (CMS-0223971 and CMS-0329416). MUSES (Materials Use: Science, Engineering, and Society) supports projects that study the reduction of adverse human impact on the total interactive system of resource use, the design and synthesis of new materials with environmentally benign impacts on biocomplex systems, as well as the maximization of efficient use of materials throughout their life cycles.

References

[1] V.C. Li, ECC — tailored composites through micromechanical modeling, Fiber Reinforced Concrete: Present and the Future, Banthia et al, CSCE, Montreal, 1998, pp. 64–97.
[2] V.C. Li, On Engineered Cementitious Composites (ECC) — a review of the material and its applications, Advanced Concrete Technology 1 (3) (2003) 215–230.
[3] V.C. Li, S. Wang, C. Wu, Tensile strain-hardening behavior of PVA–ECC, ACI Materials Journal 98 (6) (2001) 483–492.
[4] M. Şahmaran, V.C. Li, De-icing salt scaling resistance of mechanically loaded Engineered Cementitious Composites, Cement and Concrete Research 37 (7) (2007) 1035–1046.
[5] M. Şahmaran, M. Li, V.C. Li, Transport properties of Engineered Cementitious Composites under chloride exposure, ACI Materials Journal 104 (6) (2007) 604–611.
[6] M. Şahmaran, V.C. Li, Durability of mechanically loaded Engineered Cementitious Composites under high alkaline environment, Cement and Concrete Composites 30 (2) (2008) 72–81.
[7] M. Şahmaran, V.C. Li, C. Andrade, Corrosion resistance performance of steel-reinforced Engineered Cementitious Composites beams, ACI Materials Journal 105 (3) (2008) 243–250.
[8] M. Şahmaran, V.C. Li, Influence of microcracking on water absorption and sorptivity of ECC, Materials and Structures 42 (5) (2009) 593–603.
[9] M. Li, M. Şahmaran, V.C. Li, Effect of cracking and healing on durability of Engineered Cementitious Composites under marine environment, HPFRCC 5 — High Performance Fiber Reinforced Cement Composites, Stuttgart, Germany, 10–13, 2007, pp. 313–322.
[10] V.C. Li, G. Fischer, Y.Y. Kim, M. Lepech, S. Qian, M. Weimann, S. Wang, Durable link slabs for jointless bridge decks based on strain-hardening cementitious composites, Report for Michigan Department of Transportation RC-1438, 2003.
[11] M. Lepech, V.C. Li, Water permeability of cracked cementitious composites, Proceedings of Eleventh International Conference on Fracture, Turin, Italy, 2005, pp. 20–25.
[12] V.C. Li, T. Horikoshi, A. Ogawa, S. Torigoe, T. Saito, Micromechanics-based durability study of Polyvinyl Alcohol Engineered Cementitious Composite (PVA–ECC), ACI Materials Journal 101 (3) (2004) 242–248.
[13] E.H. Yang, Y. Yang, V.C. Li, Use of high volumes of fly ash to improve ECC mechanical properties and material greenness, ACI Materials Journal 104 (6) (2007) 620–628.
[14] S. Wang, V.C. Li, Engineered Cementitious Composites with high-volume fly ash, ACI Materials Journal 104 (3) (2007) 233–241.
[15] V.C. Li, C. Wu, S. Wang, A. Ogawa, T. Saito, Interface tailoring for strain-hardening PVA–ECC, ACI Materials Journal 99 (5) (2002) 463–472.
[16] AASHTO T 259-80, Standard Method of Test for Resistance of Concrete to Chloride Ion Penetration, AASHTO, USA, 2001.
[17] AASHTO T 260-97, Standard Method of Test for Sampling and Testing for Chloride Ion in Concrete and Concrete Raw Materials, AASHTO, USA, 2001.
[18] J. Crank, The Mathematics of Diffusion, 2nd edition, Oxford University Press, London, 1975.
[19] S. Chatterji, On the applicability of Fick's second law to chloride ion migration through portland cement concrete, Cement and Concrete Research 25 (2) (1995) 299–303.
[20] ASTM C1202, Standard Test Method for Electrical Indication of Concrete's Ability to Resist Chloride Ion Penetration, American Society for Testing and Materials, West Conshohocken, Pa, 2002.
[21] ASTM C1585, Standard Test Method for Measurement of Rate of Absorption of Water by Hydraulic-Cement Concretes, American Society for Testing and Materials, West Conshohocken, Pa, 2004.
[22] Y. Yang, M.D. Lepech, V.C. Li, Self-healing of ECC under cyclic wetting and drying, Proceedings of Int'l Workshop on Durability of Reinforced Concrete Under Combined Mechanical and Climatic Loads, Qingdao, China, 2005, pp. 231–242.
[23] P.S. Mangat, K. Gurusamy, Chloride diffusion in steel fibre reinforced marine concrete, Cement and Concrete Research 17 (3) (1987) 385–396.
[24] A. Konin, R. Francois, G. Arliguie, Penetration of chlorides in relation to the microcracking state into reinforced ordinary and high strength concrete, Materials and Structures 31 (209) (1998) 310–316.
[25] C.L. Page, N.R. Short, A. El Tarras, Diffusion of chloride ions in hardened cement paste, Cement and Concrete Research 11 (3) (1981) 395–406.
[26] P.F. McGrath, R.D. Hooton, Influence of binder composition on chloride penetration resistance of concrete, Proceedings of the Fourth International Conference on Durability of Concrete, Sydney, ACI SP-170, vol. (1), 1997, pp. 331–348.
[27] M. Ismail, A. Toumi, R. François, R. Gagné, Effect of crack opening on the local diffusion of chloride in cracked mortar samples, Cement and Concrete Research 38 (8–9) (2008) 1106–1111.
[28] U. Wiens, P. Schiessl, Chloride binding of cement paste containing fly ash, paper 4-iv-016 in Proceedings of the 10th International Congress on the Chemistry of Cement, Vol. 4, SINTEF, Trondheim, Norway, 1997.
[29] ACI Committee 232.2R-96, Use of Fly Ash in Concrete, American Concrete Institute, Farmington Hills, Mich., 1996, p. 34.
[30] M. Şahmaran, İ.Ö. Yaman, M. Tokyay, Development of high volume low-lime and high-lime fly-ash-incorporated self consolidating concrete, Magazine of Concrete Research 59 (2) (2007) 97–106.
[31] M.H. Shehata, M.D.A. Thomas, R.F. Bleszynski, The effect of fly ash composition on the chemistry of pore solution, Cement and Concrete Research 29 (12) (1999) 1915–1920.
[32] A.M. Neville, Properties of Concrete, Fourth edition, Longman Group Limited, 1995.
[33] S. Tsivilis, J. Tsantilas, G. Kakali, E. Chaniotakis, A. Sakellariou, The permeability of portland limestone cement concrete, Cement and Concrete Research 33 (9) (2003) 1465–1471.
[34] P. Chindaprasirt, C. Jaturapitakkul, T. Sinsiri, Effect of fly ash fineness on compressive strength and pore size of blended cement paste, Cement and Concrete Composites 27 (4) (2005) 425–428.
[35] T.U. Mohammed, T. Yamaji, H. Hamada, Microstructures and interfaces in concrete after 15 years of exposure in tidal environment, ACI Materials Journal 99 (4) (2002) 352–360.
[36] M. Kuroda, T. Watanabe, N. Terashi, Increase of bond strength at interfacial transition zone by the use of fly ash, Cement and Concrete Research 30 (2) (2000) 253–258.
[37] P.K. Mehta, P.J.M. Monteiro, Concrete: Structure, Properties, and Materials, Third Edition, McGraw Hill, New York, 2006.
[38] ASTM C 511, Standard Specification for Moist Cabinets, Moist Rooms, and Water Storage Tanks Used in the Testing of Hydraulic Cements and Concretes, vol. 04, No. 02, American Society for Testing and Materials, West Conshohocken, PA, 2002.